MAX-PLANCK-INSTITUT FÜR PLASMAPHYSIK

GARCHING BEI MÜNCHEN

Combined n = 0 and n ≠ 0 MHD Stability Analysis of Surface Current Model Tokamaks and Spheromaks

E. Rebhan[+)], A. Salat

IPP 6/190 November 1979

+)
Institut für Theoretische Physik,
Universität Düsseldorf, 4000 Düsseldorf

Die nachstehende Arbeit wurde im Rahmen des Vertrages zwischen dem Max-Planck-Institut für Plasmaphysik und der Europäischen Atomgemeinschaft über die Zusammenarbeit auf dem Gebiete der Plasmaphysik durchgeführt.

6/190 E. Rebhan, A. Salat

Combined n = 0 and n ≠ 0 MHD Stability Analysis of Surface Current Model Tokamaks and Spheromaks

November 1979
(in English)

Abstract

For a surface current model of axisymmetric equilibria with constant plasma pressure, the energy principle is used to perform a combined stability analysis of axisymmetric and nonaxisymmetric MHD modes. An improper treatment of the n ≠ 0 modes at low aspect ratio found in the literature is pointed out and corrected. In the tokamak regime, for fixed values of the aspect ratio and ß poloidal, ß is maximized by optimizing the plasma shape, while the requirements of full MHD stability are observed. In the spheromak regime, the dependence of ß on the aspect ratio and ß poloidal is considered for circular and D-shaped configurations, full MHD stability again being observed.

1. INTRODUCTION

For the surface current model (SCM) of tokamaks with constant plasma pressure, the stability with respect to ideal MHD modes has been extensively studied. A list of representative papers is given in Refs. /1-15/. Further references are available in Ref. /11/. In all of these, either only axisymmetric modes ($n = 0$) or only nonaxisymmetric modes ($n \neq 0$) have been considered.

In Ref. /16/ we pointed out a decisive qualitative difference between $n = 0$ and $n \neq 0$ modes; the critical shape of the plasma cross-section is essentially determined by $n = 0$ instabilities, $n \neq 0$ modes being of little importance, while the critical β is essentially determined by $n \neq 0$ instabilities, $n = 0$ modes having almost no influence. Unfortunately, in search of large -β configurations the requirement for $n \neq 0$ stability leads to $n = 0$ unstable plasma shapes. For clarity, we again bring in Fig. 1 the illustrative example of Ref. /16/. There, for elliptical plasma cross-sections the stability boundaries for $n = 0$ and $n \neq 0$ modes (the latter being corrected according to Section 3) are shown in a diagram β versus elongation e (see eq. (2.8) for definition). For each type of mode the stable domain is shaded. Complete stability prevails only in the doubly shaded area. The largest critical β compatible with full stability is obtained at the intersection

between the two stability boundaries and is significantly smaller than the largest critical ß obtained from a pure $n \neq 0$ analysis.

If one wants to manage without great technical outlay such as feedback stabilization, one is thus forced to regard both $n = 0$ and $n \neq 0$ modes. Owing to the rather rough approximation to realistic experiments which is provided by the SCM, the use of SCM stability analysis lies less in its application to a specific single situation, but consists rather in the possibility of doing extensive parameter studies in order to find out qualitative trends. The purposes of this paper are therefore a study in parameter space, looking for completely MHD stable configurations which have as large as possible ß values, and comparison of these with more simple standard configurations. Since many instabilities occuring in more realistic plasma models are, in principle, absent in the sharp boundary model, it is tempting to consider the ß values thus obtained as upper bounds for realistic configurations.

In Section 2, we give a short review of SCM equilibrium properties and definitions as far as is necessary in this paper. For more details and for a description of our $n = 0$ mode analysis we refer to our previous work on SCM equilibria /13-16/.

For the $n \neq 0$ modes we adopted a method essentially due to Martensen /7, 17/. The main steps of this method consist in reducing the energy principle to a variational principle on the plasma boundary and making this problem one-dimensional by Fourier analysis with respect to the toroidal angle Θ. The remaining numerical problem is made complicated by the fact that some quantities entering the variational problem are determined by integral equations with singular kernels. Martensen overcame this complication by extraction and analytical treatment of the kernel singularities. A very compact and elegant representation of this method may be found in Ref. /11/. For discretization of the numerical problem we preferred a Fourier-analysis with respect to a poloidal coordinate on the plasma surface like Freidberg et al. rather than using trigonometric interpolation like Martensen. The poloidal coordinate we used is the "adapted coordinate" described in Ref. /16/.

In redoing the $n \neq 0$ mode analysis we found that some of the results published in the fusion-oriented literature /11-12/ are not quite correct. To a certain degree, this necessitated a revision of the $n \neq 0$ stability results since, on the other hand, the work of Martensen et al. /7-8, 17/ contains only very few numerical results. This revision is carried out in Section 3.

In Section 4, we present results of a ß maximization in the tokamak regime. This was done for fixed A and $ß_p$ by optimization of the plasma shape while observing the requirements of full MHD stability.

Finally, in Section 5 we consider configurations of the spheromak type, again observing the requirements of full MHD stability.

2. SCM EQUILIBRIUM PROPERTIES AND DEFINITIONS

In the following, R is the perpendicular distance of a point from the axis of rotational symmetry, $\vec{e}_\theta$ is a toroidal unit vector and $\vec{e}_p$ is a poloidal unit vector tangential to the plasma surface. With the dimensionless units of Ref. /13/, the magnetic fields inside and outside the plasma respectively are

$$\vec{B}_{pl} = \frac{\Lambda_p}{R}\,\vec{e}_\theta \quad , \qquad \vec{B}_v = \frac{\Lambda_v}{R}\,\vec{e}_\theta + B\,\vec{e}_p \quad , \tag{2.1}$$

where

$$B = \frac{1}{R}\left[1 + \beta_p\,(R^2 - 1)\right]^{1/2}, \tag{2.2}$$

Λ_p , Λ_v are constants and $\beta_p = p/(\frac{B_o^2}{2})$, B_o being the poloidal field strength on the plasma surface at $R = (R_{min} + R_{max})/2 = 1$; β_p is related to Λ_p and Λ_v by

$$\beta_p = 1 + \Lambda_v^2 - \Lambda_p^2 \quad . \tag{2.3}$$

The safety factor q is given by

$$q = \Lambda_v \frac{q_g}{A} \quad , \qquad q_g = \frac{A}{2\pi} \oint \frac{d\ell}{R^2 B} \quad , \tag{2.4}$$

$d\ell$ being the arc length along a poloidal cut of the plasma surface. With the definition

$$\beta = p/\left(p + \frac{1}{2} B_{pl}^2 \Big|_{R=1}\right) = p/\left(\frac{1}{2} B_{vo}^2\right), \qquad (2.5)$$

where B_{vo} is the vacuum field strength on the plasma surface at R = 1, we have

$$\beta = \beta_p / (1 + \Lambda_v^2) . \qquad (2.6)$$

Our definition of the aspect ratio A is

$$A = (R_{max} + R_{min})/(R_{max} - R_{min}), \qquad (2.7)$$

where $R_{max}(R_{min})$ is the largest (smallest) distance of the plasma surface from the axis of symmetry. With z being a coordinate along this (z = 0 on the equatorial plane), our definition of elongation is[1)]

$$e = (z_{max} - z_{min})/(R_{max} - R_{min}), \qquad (2.8)$$

where $z_{max} = -z_{min}$ is the largest distance of the plasma surface from the equatorial plane. The D-shapes we shall consider are given by

$$e^2(R-1)^2 + [1 - 2A(R-1)\tau_3 + \tau_3^2]z^2 = e^2/A^2, \qquad (2.9)$$

τ_3 being a measure of the triangularity. Finally, in Section 4 we shall consider very general plasma shapes represented by

$$s = c\left[1 + \sum_{n=1}^{N} c_n \cos n u\right], \qquad (2.10)$$

where

$$s = [(R-1)^2 + z^2]^{1/2}, \qquad u = \text{arc tg}\left(\frac{z}{R-1}\right).$$

---

1) As for the definition of e, Fig. 1 in Ref. /13/ contains a mistake.

3. REVISION OF THE n ≠ 0 MODES

a) The proper boundary condition

Among the papers on n ≠ 0 mode MHD stability for SCM tokamaks, Ref. /11/ contains by far the most and most general results and was therefore most suitable for testing our n ≠ 0 mode code. We find rather good agreement of results at large A which, however, deteriorates as A decreases. Typical relative deviations are ≈ 3 % at A = 10 and ≈ 15 % at A = 2, a difference in the definitions of β_p and β being taken into account. Closer inspection showed that Ref. /11/ contains an improper treatment of the boundary condition between the plasma and vacuum. Since it appears that this boundary condition is a pitfull into which one frequently stumbles, we give a short derivation of the proper condition. Its original form is well known and reads

$$\vec{n} \times \vec{A} = - \left(\vec{\xi} \cdot \vec{n} \right) \vec{B}_v \quad , \tag{3.1}$$

where

$$\vec{n} = \frac{\nabla \Psi}{|\nabla \Psi|} \quad , \qquad \nabla \Psi = RB \left(\vec{e}_p \times \vec{e}_\theta \right) \quad , \qquad \delta \vec{B}_v = \nabla \times \vec{A} \quad . \tag{3.2}$$

Multiplying eq. (3.1) by $\nabla \Psi$ and taking its divergence, we get

$$\nabla\Psi \cdot \delta\vec{B}_v = \vec{B}_v \cdot \nabla (\vec{\xi} \cdot \nabla\Psi) . \qquad (3.3)$$

Using eqs. (2.1), (3.2) and $\vec{e}_p \cdot \nabla = \partial/\partial\ell$, we finally get

$$\vec{n} \cdot \delta\vec{B}_v = \frac{\Lambda_v}{R^2} \frac{\partial}{\partial\theta} (\vec{\xi} \cdot \vec{n}) + \frac{1}{R} \frac{\partial}{\partial\ell} [R B (\vec{\xi} \cdot \vec{n})] . \qquad (3.4)$$

Instead of the last term in eq. (3.4), Ref. /11/ has $\frac{\partial}{\partial\ell} [B (\vec{\xi} \cdot \vec{n})]$, which becomes correct for $A \to \infty$.

b) Consideration of the $n \geq 1$ modes

It is claimed in Ref. /11/ that $n = 1$ is the worst among the $n \neq 0$ modes. Analytic results for $A = \infty$ /9-10/ are given as a reason for this, where n enters only in the combinations β/n^2, qn and β/n and may thus be scaled out completely in the marginal case. Obviously, this argument does not hold for $A < \infty$ (e.g. see formula (A2) in Ref. /11/), and we therefore also did calculations for $n > 1$.

A difficulty met in these calculations should be pointed out. Certain quantities entering the kernels of the integral equations mentioned in the introduction are defined by a trinomial linear recursion with respect to n (see formulae (167)-(168) in Ref. /17/). It is just the

minimal solution of this recursion which is needed and this is unstable. A numerically stable but arkward method of calculations consist in breaking off a representation of the solution which uses continued fractions /18/. In our code, we evaluated a representation by means of the hypergeometric function. Specifically, we used /19/

$$\int_0^{2\pi} d\psi \frac{\cos n\psi}{[1-2z\cos\psi+z^2]^{\alpha}} = \frac{2\pi z^n \Gamma(\alpha+n)}{n!\,\Gamma(\alpha)} {}_2F_1(\alpha, \alpha+n; 1+n; z^2)$$

Since the claim of Ref. /11/ is correct for $A = \infty$, a different result could only be expected at low aspect ratio. However, for all low A cases which we have calculated, it was confirmed that marginal stability is determined by the n = 1 mode. Representative examples are given in Figs. 2 and 3. For elliptical cross-sections, $A = 2$ and $\beta_p = 1$, Fig. 2 shows the critical q as a function of elongation for n = 1, 2, 3. For a specific elongation, Fig. 3 shows the critical q as a function of the mode number n. Further calculations for circular, D-shaped and doublet-shaped cross-sections as well as all situations met in Sections 4 and 5 showed the same behaviour. However, we cannot exclude that there may exist regions in parameter space where modes with $n > 1$ take over. Moreover, our investigation is limited to $n \lesssim 30$.

Considering situations beyond the boundary of marginal stability, we found that higher n-modes may well become more unstable than the n = 1 mode in the sense that $\delta^2 W$ becomes more negative. $n > 1$ calculations at low aspect

ratio are also presented in Ref. /12/ for circular shapes. We found agreement with our results only for n = 1. For n > 1 we could not track down a reason for the discrepancies since Ref. /12/ contains too many misprints and inconsistencies.

c) Testing of the numerical code

In view of the hidden pitfalls in the problem under consideration, it was important to find conclusive tests for our code. Since our method of testing can also be applied in treating the perturbational vacuum field of diffused current model (DCM) equilibria, we give a short outline of it here.

The trivial comparison with analytical results for $A = \infty$ needs no further explanation. Considering low A cases, by far the most extensive part of all calculations consists in solving the integral equations mentioned in the Introduction. After discretization, they may be put in the form

$$\psi_\ell = \sum_m A^{(n)}_{\ell m} \, (n \cdot \nabla\psi)_m \quad , \tag{3.5}$$

where $\nabla\psi = \delta B$ is a vacuum field which has no singularities either inside or outside the plasma, and where ψ_ℓ and $(n \cdot \nabla\psi)_\ell$

are the poloidal Fourier components of ψ and $(\vec{n}\cdot\nabla\psi)$ respectively. This problem is met for both the plasma and the vacuum contribution to $\delta^2 W$. Calculating the coefficients $A_{\ell m}^{(n)}$ for the plasma and vacuum contributions, respectively, is the key problem of the $n \neq 0$ stability analysis.

Any vacuum potential $\psi = \psi_o(R,z)e^{in\Theta}$ which has no singularities inside (outside) the plasma as far as the plasma (vacuum) contribution to $\delta^2 W$ is concerned must satisfy the corresponding equation (3.5). One can therefore test the coefficients $A_{\ell m}^{(n)}$ by inserting known solutions ψ into eq. (3.5). Simple known solutions, e.g. for the vacuum contribution which we have used, may be found in Ref. /20/. A last test (only for $n = 1$) consisted in a temporary use of the improper boundary condition of Ref. /11/ and led to complete agreement of results.

4. ß-MAXIMIZATION BY SHAPE OPTIMIZATION IN THE TOKAMAK REGIME

For comparison we first consider circular and elliptical plasma cross-sections. For both Fig. 4 shows with fixed $ß_p$ the largest ß compatible with complete MHD stability as a function of 1/A. The curve for elliptical cross-sections was obtained according to Fig. 1. The corresponding q values are given in Fig. 5.

We now come to this optimization problem. In a previous paper /16/ we considered plasma shapes represented by eq. (2.10) for $N \lesssim 12$. Employing a modification of the method of steepest descent, we determined the coefficients c_n for fixed values of A and $ß_p$ such that ß became as large as possible while stability with respect to n = 0 modes was still observed. $n \neq 0$ modes were rather crudely treated by requiring that q = 1. We had some arguments for the assumption that this way the optimum shape is determined rather accurately while the maximum ß value necessarily remains largely undetermined. Increasing N beyond $N \approx 10$ brought no more visible change of the optimum shape.

As a last step prior to full optimization we now calculated the formerly undetermined value of critical ß for the shapes previously obtained, using now our $n \neq 0$ code. The result of this calculation is represented by the solid curve in Fig. 4.

For complete optimization, q must be added to the list of variable parameters while n = 0 and n ≠ 0 mode stability must be simultaneously observed during the optimization procedure described in Ref. /16/. Since this full optimization is rather time-consuming, we did it only for two A values. The result is given by the crosses in Fig. 4. For A = 4, the result is imperceptibly above the solid curve, while the corresponding optimum shape (Fig. 6a) differs imperceptibly from the optimum shape obtained for fixed q = 1. For A = 3.8, in the process of optimization a constriction of the plasma boundary develops, forming a doublet-like plasma shape as in the q = 1 case. This constriction becomes more and more pronounced until the large curvature at the centre of the constriction causes numerical problems and the optimization procedure must be stopped before it comes to an end. The cross at A = 3.8 in Fig. 4 belongs to the intermediate stable shape shown in Fig. 6b. The ß gain due to the plasma constriction is much less than it is in the q = 1 optimization since q rises from 1.55 to 1.79 when going from the unconstricted to the constricted shape.

These results confirm to an almost unexpected degree our previous assumption about the optimization with fixed q = 1, and we may consider practically the whole of the solid curve as the result of a complete optimization.

5. MHD STABILITY BOUNDARIES IN THE SPHEROMAK REGIME

In Ref. /21/, the first theoretical study of magnetic vacuum confinement of tokamaks at the lower limit of the aspect ratio is found, allowing of pure poloidal field confinement. For the latter case there has recently been a revival of interest, and for corresponding configurations the name "Spheromak" has been proposed (see /22-23/, where a list of further references is found).

Let us first consider the concept of an "ideal spheromak" in the frame work of the SCM. Since the confining vacuum field should be purely poloidal, from eqs. (2.1) and (2.3) - (2.6) we get the requirements

$$\Lambda_v = 0 , \qquad \beta_p \leq 1 , \qquad q = 0 \tag{5.1}$$

and

$$\beta = \beta_p \ . \tag{5.2}$$

Numerical calculations show that there exists no MHD stable ideal SCM spheromak. We may look, however, for configurations which come close to the ideal spheromak, expecting that ideal DCM spheromaks of similar shape will show qualitatively similar stability behaviour as far as the most dangerous external MHD gross modes are concerned. To a certain degree this expectations will be confirmed by a comparison with DCM calculations (see below).

Let us first consider circular plasma cross-sections. Figure 7 shows the critical ß as a function of $ß_p$ for several fixed values of A. Coming from large A, with decreasing A we first get increasingly better approximation to the ideal spheromak line $ß = ß_p$. For fixed low $A \gtrsim 1.05$, from ß = 0 up to the maximal ß this approximation is relatively uniform and of acceptable quality, deteriorating appreciably after $ß_p$ is increased above the value which corresponds to the maximal ß. Below $A \approx 1.05$ the approximation gets worse with further decreasing A as is demonstrated by A = 1.01. For some A values between 1.3 and 1.01 the corresponding marginal curves are shown in Fig.8, being restricted to the neighbourhood of their maximum in order not to destroy the clearness of the figure. The position of these maxima is shown in addition, $A \approx 1.05$ having the closest approach to $ß = ß_p$. A discussion of the deterioration below $A \approx 1.05$ will be given later.

In a similar diagram (Fig. 9) we consider D shaped cross-sections ($\tau_3 = -0.6$, see eq. (2.9)) with different elongation, all having the same aspect ratio A = 1.1. For comparison, also the corresponding curve for a circle ($\tau_3 = 0$, e = 1) is taken over from Fig. 7. Beyond $ß_p \approx 0.3$, of all cases shown the D-shape with largest elongation is most favourable; for $ß_p \lesssim 0.3$ circular shape is equivalent. For e = 1, a circular shape is more favourable than the

corresponding D-shape. It is interesting to note that the relative deviation $(\beta_p - \beta)/\beta_p$ from the ideal spheromak is smallest close to the maximal β for almost all curves shown.

We shall now try a rough qualitative comparison of our results with MHD-stability results obtained in Ref./22/ for DCM spheromaks, although this comparison appears problematic owing to an almost opposite approach. Since our calculations violate the condition for an ideal spheromak, they may be considered as a zero-order approximation, and a glance at Fig. 9 shows that for given A characteristic distinguishing features appear only at large β values. The DCM calculations of Ref. /22/ are certainly a better approximation. However, since an expansion about $\beta = 0$ is employed, this approach is best just for low β values.

According to these DCM calculations, elongated D-shapes ($e > 1$) are ruled out owing to internal tilting modes which are, in principle, absent in a SCM spheromak. A configuration with D-shaped plasma boundary and $b/a = 0.5$ according to definition /22/ (corresponding to values $e = 1$ and $\tau_3 \approx -0.6$ according to our definitions) is considered most favourable, yielding values of $\langle \beta^* \rangle_{coil} = \langle p^2 \rangle^{1/2} / (\frac{1}{2} B^2_{edge})$ between 13 % and 25 %, if plasma currents are excluded from a central hole.

Comparison with eq. (1.5) shows that $\langle \beta^* \rangle_{coil}$ may be identified with our β.

Comparing DCM and SCM shapes, it appears reasonable not to take the DCM plasma boundary but an internal flux surface which contains the bulk of the plasma. The e = 1 configuration, favoured in Ref. /22/, thus corresponds approximately to a SCM configuration with e = 1 and τ_3 somewhere between 0 and -0.6. According to Figs. 8 and 9 this corresponds to a maximal β somewhere between 14 % and 21,5 %, which is in quite good agreement with the DCM results.

The β gain which according to Ref. /22/ is obtained by exclusion of the plasma currents from a central hole has a SCM counterpart in the fact that, according to Fig. 7, for fixed β_p the critical β appreciably increases when a central hole is left open by raising A from $A \approx 1$ to A = 1.1. Also, according to Fig. 8 the largest possible β is obtained with A slightly above A = 1.

6. CONCLUSIONS

For a SCM model of axisymmetric equilibria with constant plasma pressure we carried out a combined $n = 0$ and $n \neq 0$ MHD stability analysis in the tokamak and spheromak regimes. For a wide range of parameters, we proved numerically that the boundary of marginal stability is determined only by $n = 0$ and $n = 1$ modes, a fact which has so far only been regarded as plausible by extrapolation from its validity at $A = \infty$.

In the tokamak regime, we maximized ß by optimizing the plasma shape with A and $ß_p$ kept fixed. For $A \gtrsim 6$, the maximum ß thus obtained is insignificantly larger than the maximum ß of elongated elliptical shapes. In the range $3.8 \lesssim A \lesssim 6$, the optimum shape looks like a combination of racetrack and D-shape, yielding an absolute ß of 5.6 % and a relative ß gain of ≈ 20 % (as compared with elliptical shape) at $A = 4$. Below $A = 3.8$, a rather small further increase of ß can be achieved by transition from a racetrack/D-shape combination to deeply notched doublet--type shapes.

In the spheromak regime it is found that an ideal SCM spheromak with zero external toroidal field is never stable. The best approximation to an ideal spheromak which at the same time allows for the largest ß is provided by

configurations with a small central hole ($A \approx 1.05$). For oblate spheromaks of plasma elongation $e = 1$, which are optimum according to DCM calculations, we obtained ß values in the range of 14 % to 21.5 %.

ACKNOWLEDGEMENT

One of the authors (E.R.) expresses his gratitude to Max-Planck-Institut für Plasmaphysik for hospitality received on several occasions during the preparation of this paper. He also expresses his thanks to Deutsche Forschungsgemeinschaft for its support of his contribution to this project.

FIGURE CAPTIONS

Fig. 1 $n = 0$ and $n \neq 0$ stability boundaries in an e-ß plane, stable regions shaded

Fig. 2 Critical q versus elongation e of elliptical plasma cross-sections for n = 1,2,3

Fig. 3 Critical q versus toroidal mode number n for an elliptical cross-section

Fig. 4 Maximum ß versus inverse aspect ratio for circular (dotted), elliptical (dashed) and optimized shape (solid)

Fig. 5 Critical q versus inverse aspect ratio, as in Fig.4

Fig. 6 Optimum shape (A = 5, Fig.a) and intermediate doublet-type shape (A = 3.8, Fig. b)

Fig. 7 Critical ß versus $ß_p$ for circular shape and different values of A, $ß = ß_p$ representing the "ideal spheromak"

Fig. 8 Critical ß versus $ß_p$, close to maxima, and ß maxima versus $ß_p$, for small A

Fig. 9 Critical ß versus $ß_p$ for the circle and various D-shapes at A = 1.1, shape qualitatively indicated for each curve.

REFERENCES

/1/ Biermann L., Hain K., Jörgens K., Lüst R., Z. Naturforschg. 12a (1957) 826

/2/ Jörgens K., Z. Naturforschg. 13a (1958) 493

/3/ Shafranov V.D., Sovj.J.Atomic Energy 1 (1956) 709

/4/ Rosenbluth M., Proc. 3rd Int.Conf.on Ion.Phen. in Gases, (Venice 1957)

/5/ Tayler R.J., Proc.Phys.Soc. London B70 (1957) 1049

/6/ Lüst R., Suydam B.R., Richtmyer R.D., Rotenberg A., Levy D., Phys. Fluids 4 (1961) 891

/7/ Martensen E., Z. Naturforschg. 17a (1962) 733

/8/ Martensen E., Sengbusch K.V., Proc. 11th Intern. Congr. of Applied Mechanics (Munich, 1964) 1010

/9/ Freidberg J.P., Haas F.A., Phys.Fluids 16 (1973) 1909

/10/ Freidberg J.P., Haas F.A., Phys.Fluids 17 (1974) 440

/11/ Freidberg J.P., Grossmann W., Phys. Fluids 18 (1975) 1494

/12/ Kito M., Honma T., J.Phys.Soc.Japan 41 (1976), 1749

/13/ Rebhan E., Salat A., Nucl.Fus. 16 (1976) 805

/14/ Rebhan E., Salat A., Nucl.Fus. 17 (1977) 251

/15/ Rebhan E., Salat A., Nucl.Fus. 18 (1978) 1431

/16/ Rebhan E., Salat A., Nucl.Fus. 18 (1978) 1639

/17/ Martensen E., Acta Math. Uppsala, 109 (1963) 75

/18/ Meixner J., Schäffke W., Mathieusche Funktionen und Sphäroidfunktionen mit Anwendungen auf physikalische und technische Probleme, Springer-Verlag Berlin (1954) pp. 89

/19/ Magnus W., Oberhettinger F., Soni R., Formulas and Theorems for the Special Functions of Mathematical Physics, Springer Verlag, Berlin (1966), p. 55

/20/ Dommaschk W., IPP-Report 0/38 (1978).

/21/ Morikawa G.K., Rebhan E., Phys. Fluids 13 (1970) 497

/22/ Bussac M.N., Furth H.P., Okabayashi M., Rosenbluth M.N., Todd A.M., PPPL Report 1472 (1978)

/23/ Rosenbluth M.N., Bussac M.N., Nucl.Fus. 19 (1979) 489.

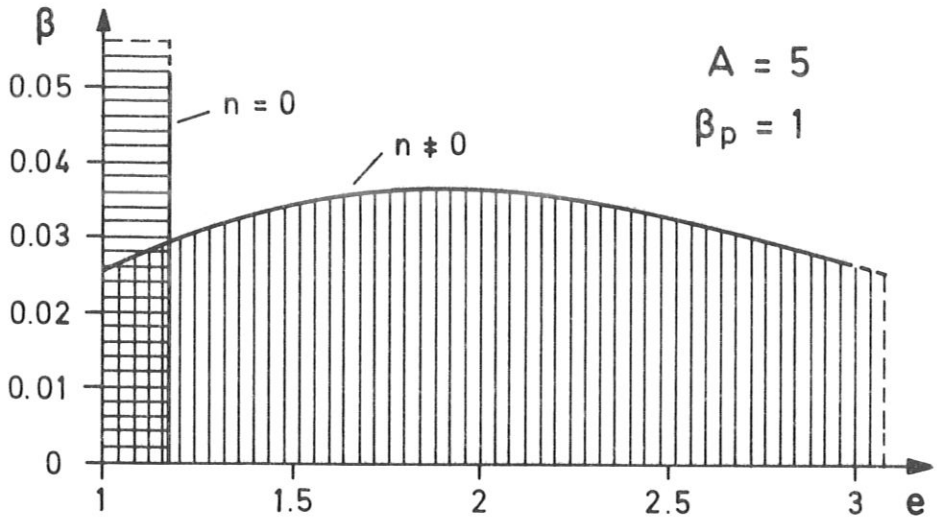

Fig. 1

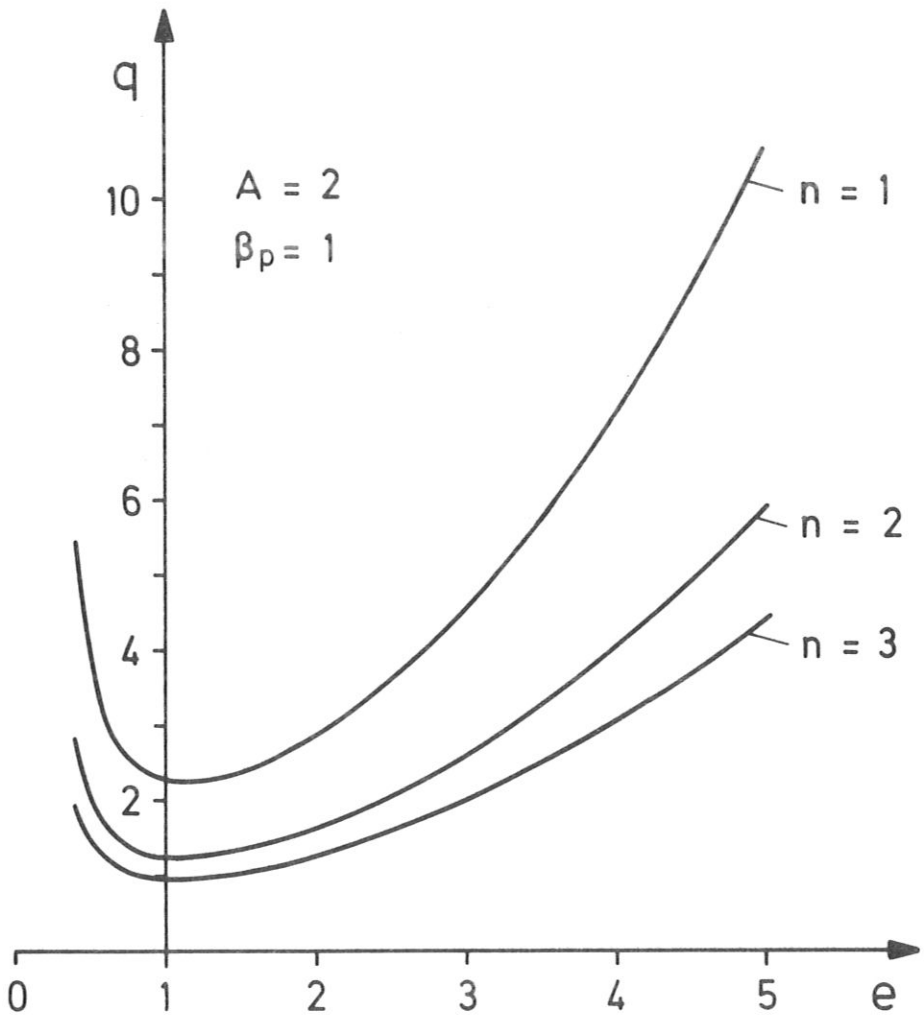

Fig. 2

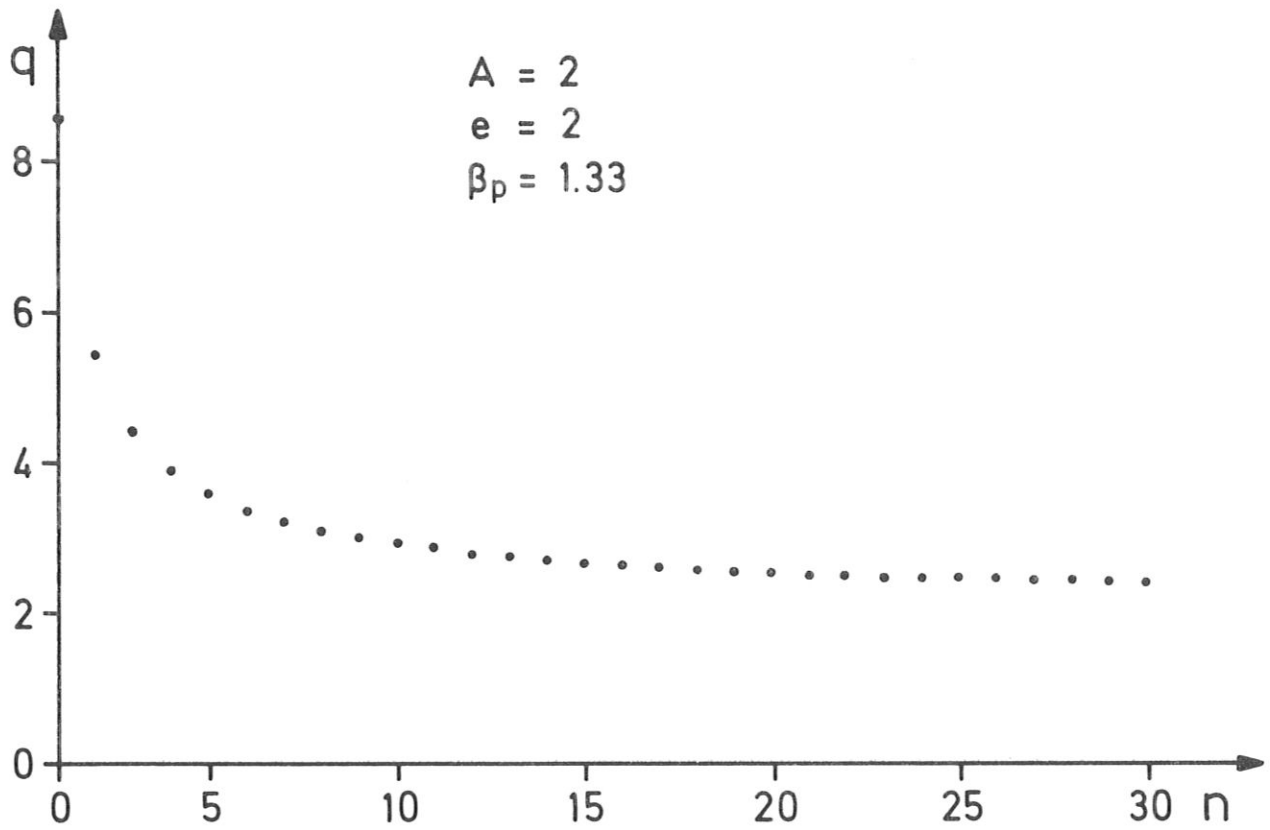

Fig. 3

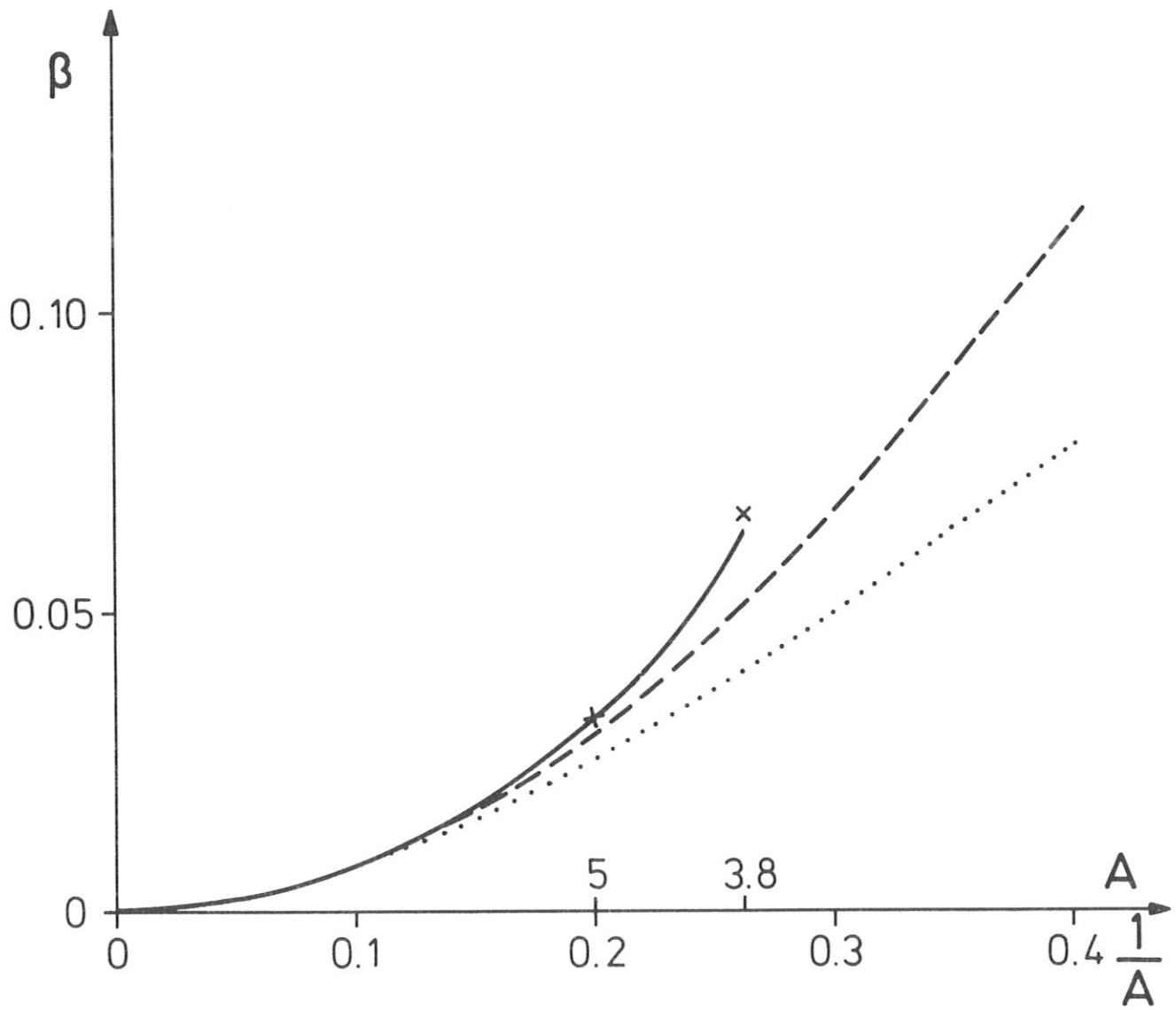

Fig. 4

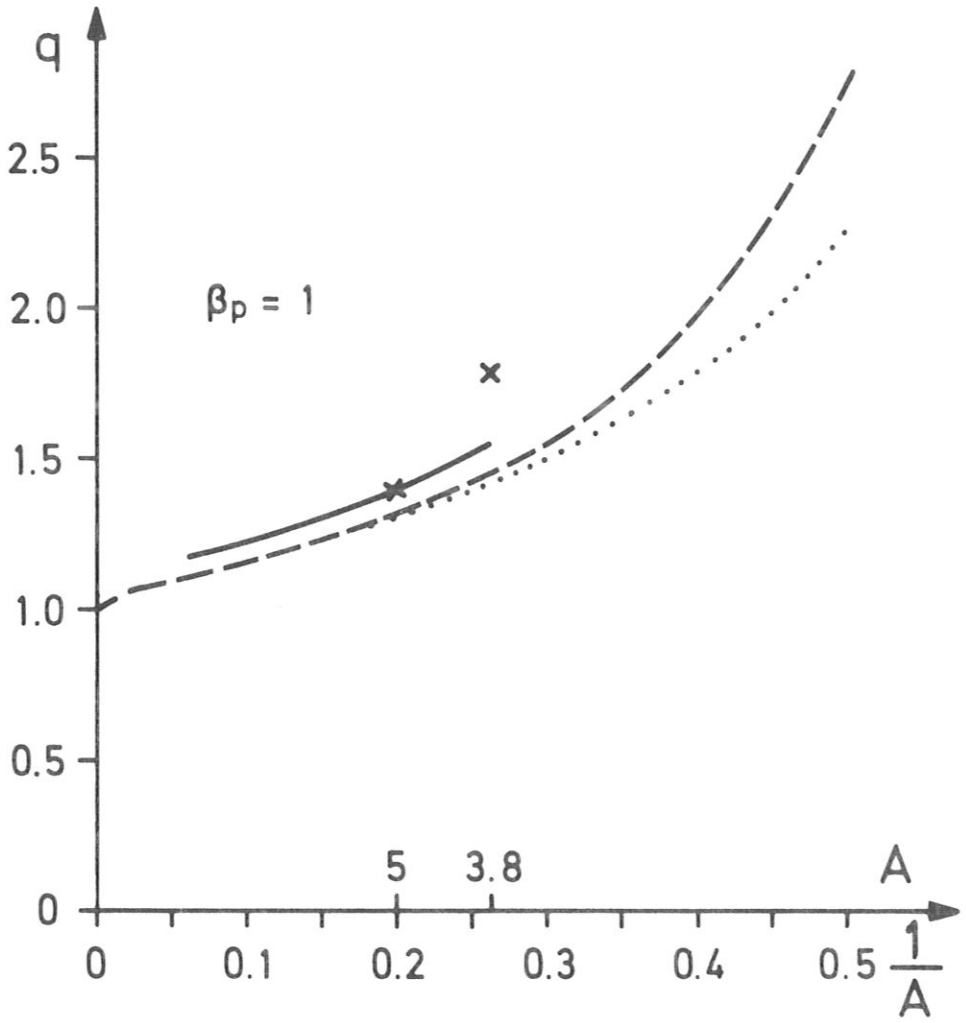

Fig. 5

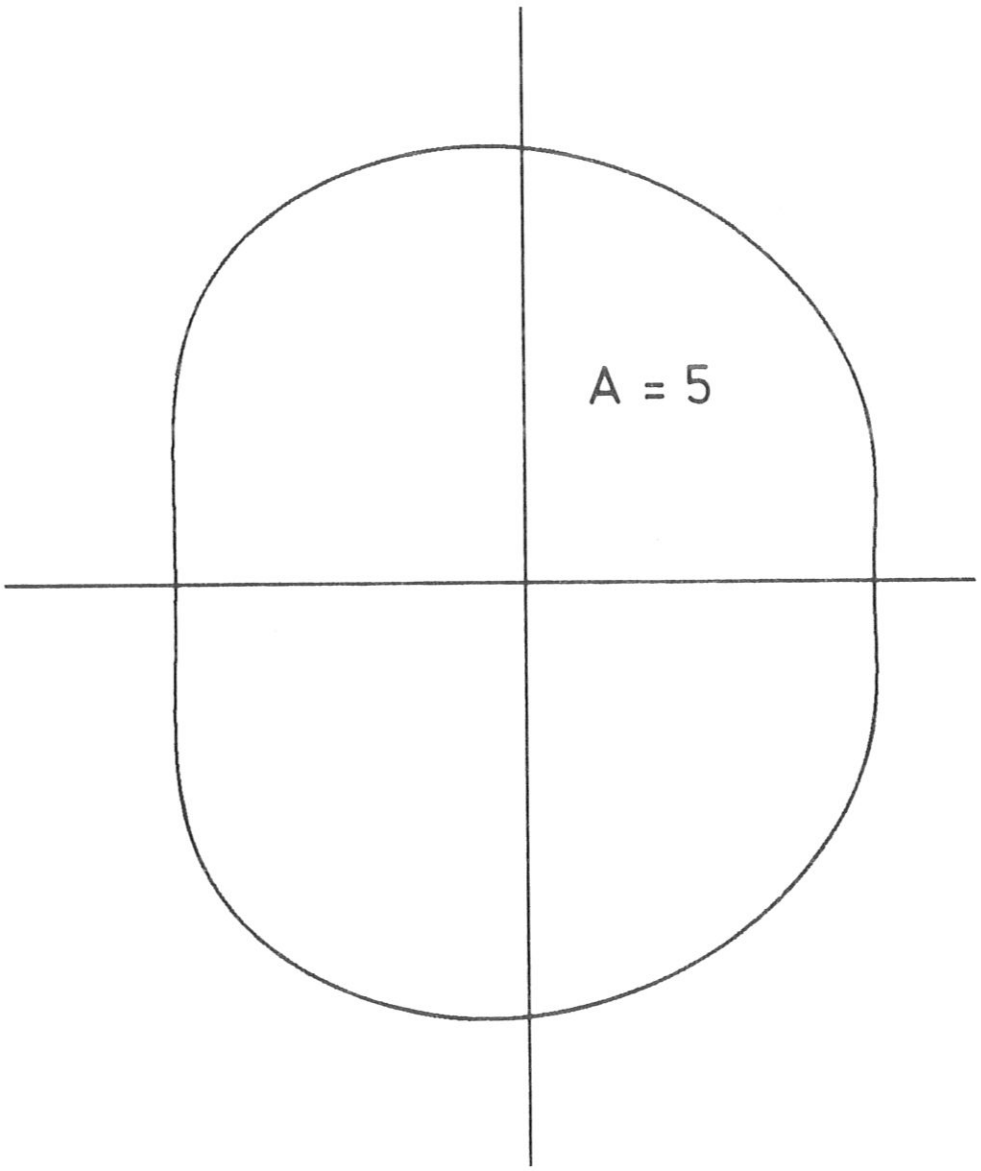

Fig. 6a

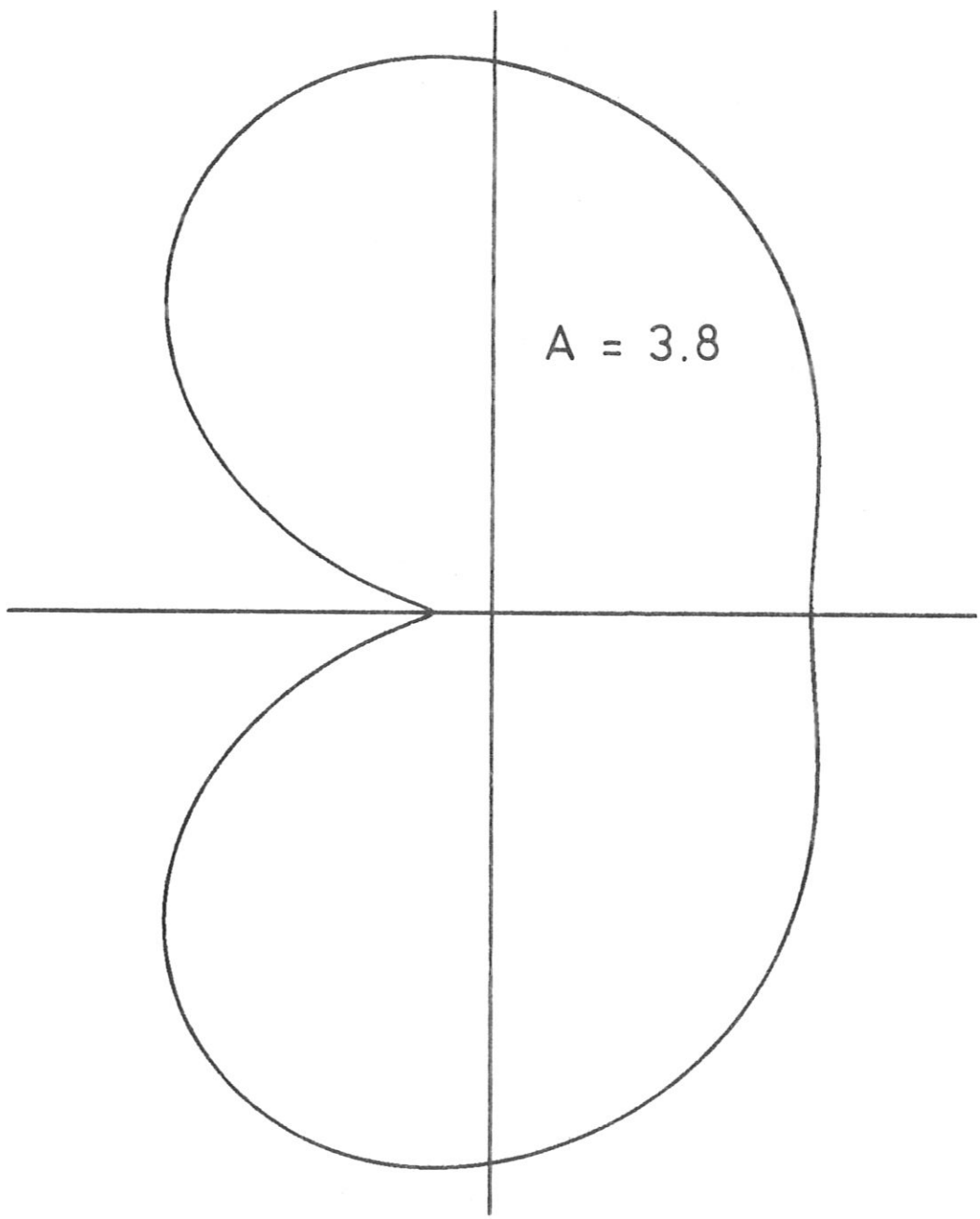

Fig. 6b

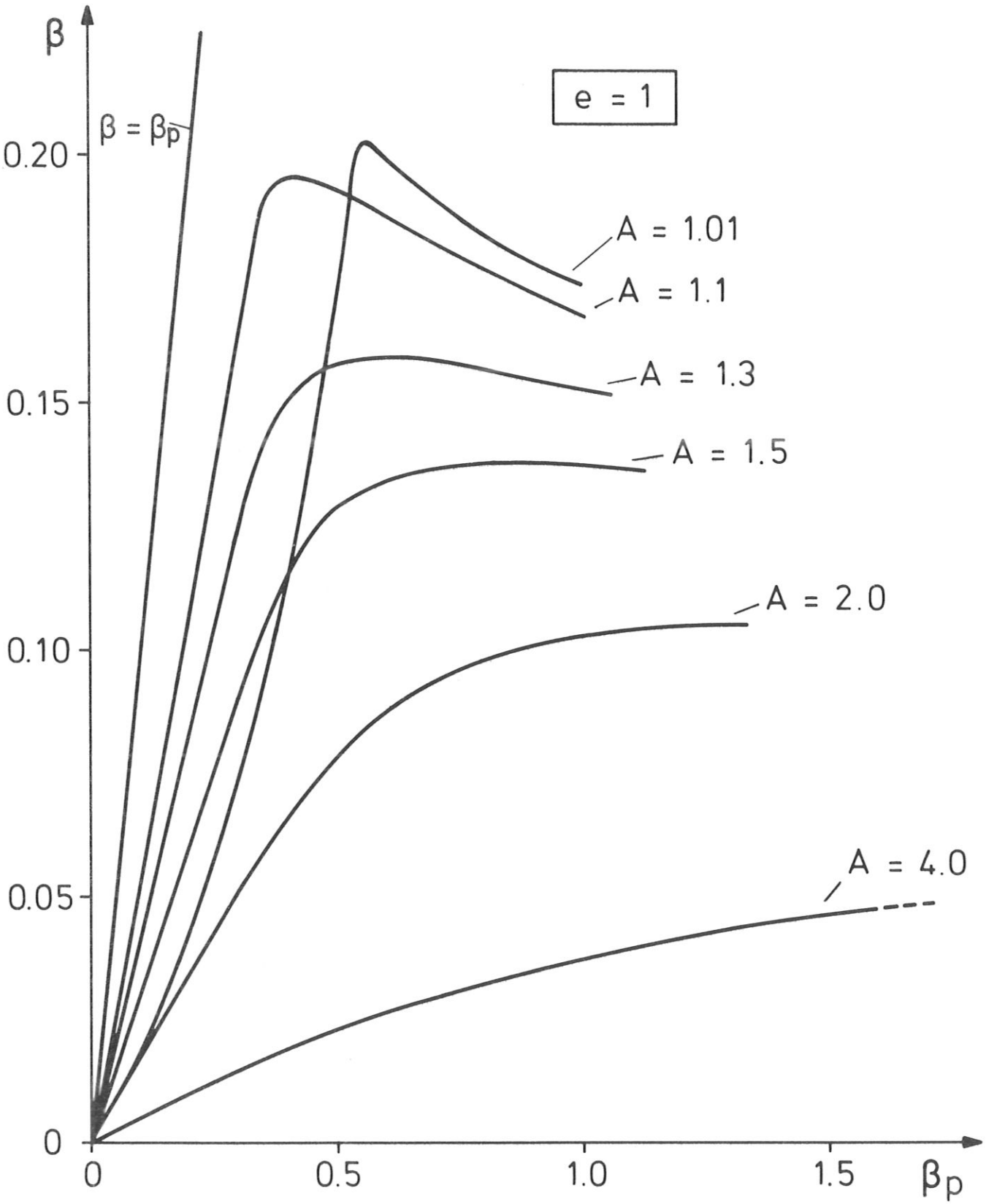

Fig. 7

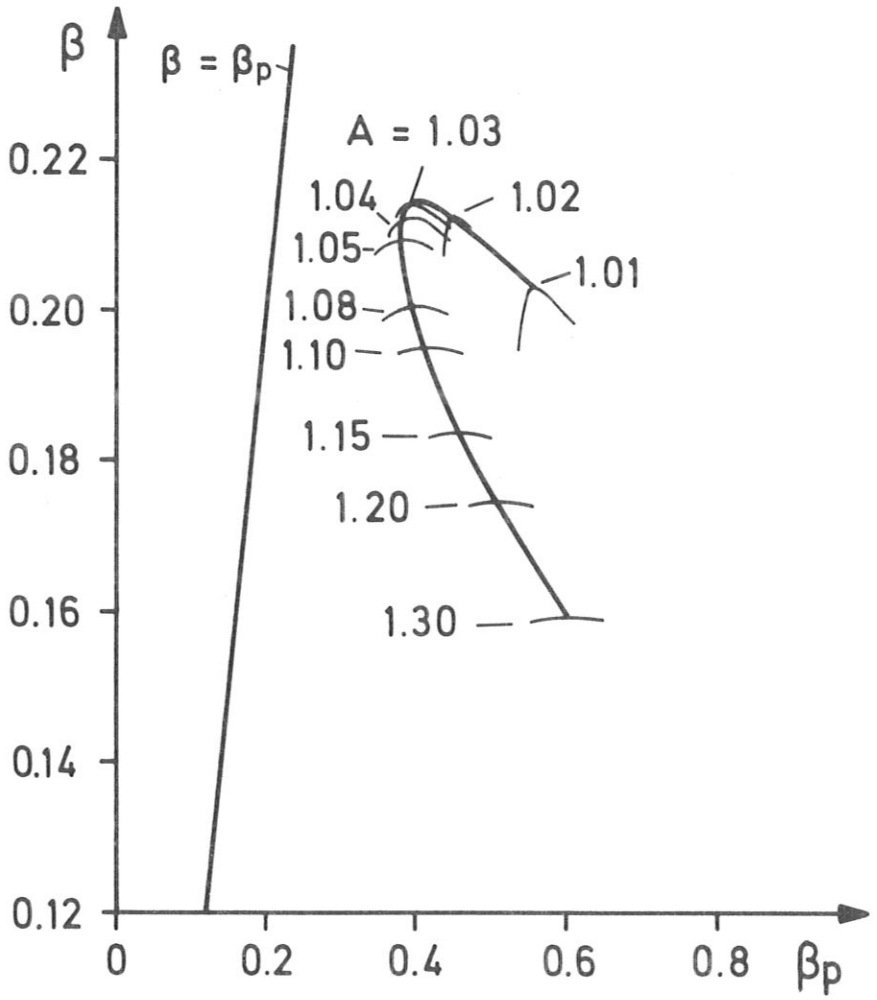
β
β = βp
A = 1.03
1.04
1.02
1.05
1.01
1.08
1.10
1.15
1.20
1.30
0.22
0.20
0.18
0.16
0.14
0.12
0
0.2
0.4
0.6
0.8
βp

Fig. 8

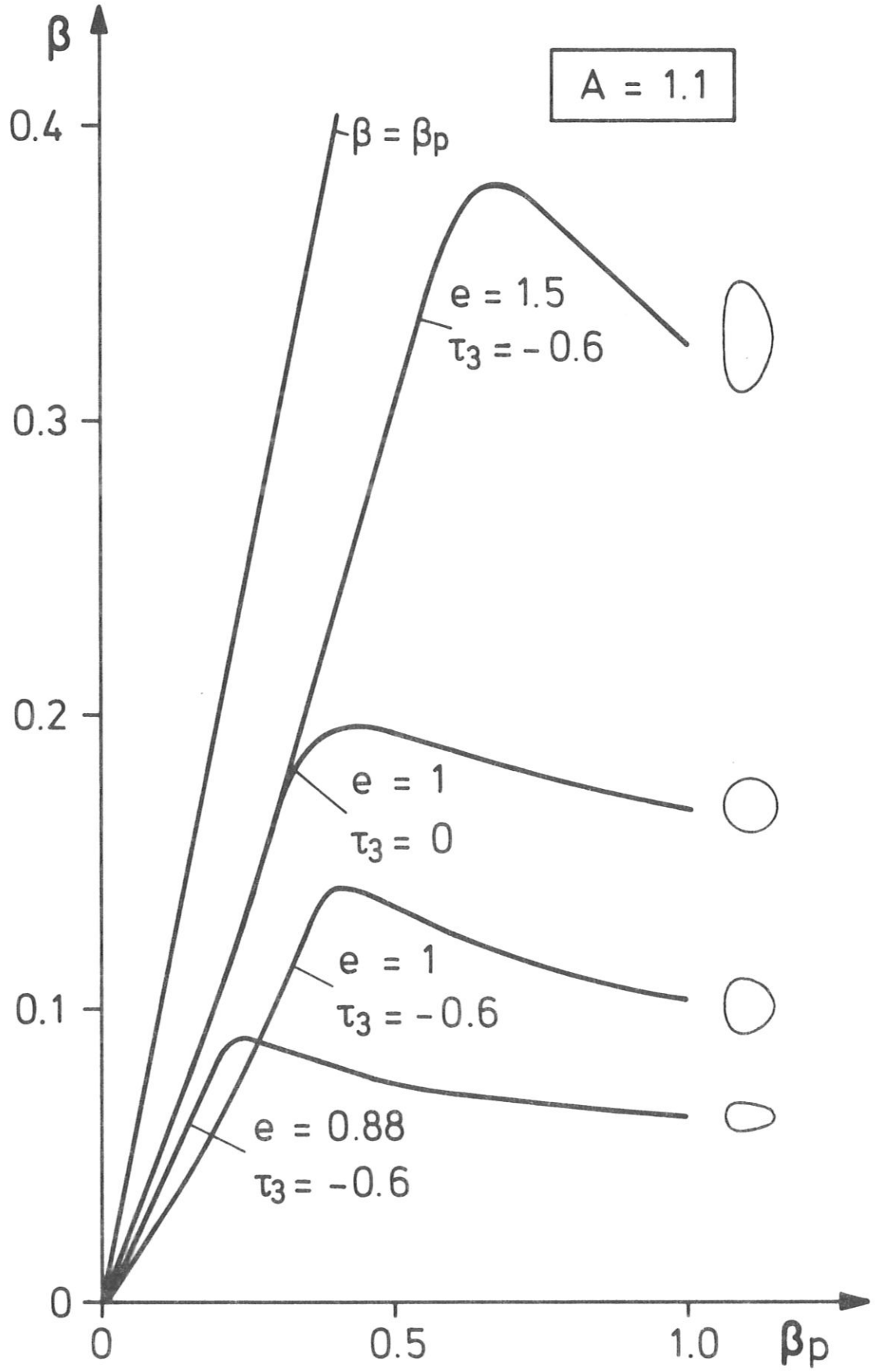

Fig. 9